Journal of Saudi Chemical Society (2022) **26**, 101491

King Saud University

Journal of Saudi Chemical Society

www.ksu.edu.sa
www.sciencedirect.com

ORIGINAL ARTICLE

Enhanced energy transfer from diolefinic laser dyes to meso-tetrakis (4-sulfonatophenyl) porphyrin immobilized on silver nanoparticles: DFT, TD-DFT and spectroscopic studies

Ahmed A. AboAlhasan [a], Mahmoud A.S. Sakr [b], Mostafa F. Abdelbar [c], Hamdy S. El-Sheshtawy [d], Samy A. El-Daly [a], El-Zeiny M. Ebeid [a,b,*], Rania Hussien Al-Ashwal [d], Sadeq M. Al-Hazmy [e]

[a] *Chemistry Department, Faculty of Science, Tanta University, Tanta, Egypt*
[b] *Misr University for Science and Technology (MUST), 6th October City, Egypt*
[c] *Institute of Nanoscience and Nanotechnology, Kafrelsheikh University, Egypt*
[d] *Advance Diagnostic and Progressive Human Care Research Group, School of Biomedical Engineering and Health Science, University Technology Malaysia, Johor, Malaysia*
[e] *Chemistry Department, College of Science, Qassim University, Qassim, Saudi Arabia*

Received 7 February 2022; revised 16 May 2022; accepted 19 May 2022
Available online 29 May 2022

KEYWORDS

Fluorescence Resonance Energy Transfer (FRET);
Silver nanoparticles;
Laser dyes;
DFT calculations;
TD-DFT calculations

Abstract Porphyrin derivatives are known singlet oxygen sensitizers in photodynamic therapy (PDT). Energy transfer from a class of diolefinic laser dyes (DOLDs) as energy donors to the sodium salt of meso-tetrakis (4-sulfonatophenyl) porphyrin (TPPS) as the accepter of energy would extend the range of photon harvesting down to the UV-region. Energy transfer was substantially enhanced in the presence of metallic silver nanoparticles (AgNPs), as revealed by steady-state emission spectroscopy, lifetimes, and quantum mechanics. DOLDs under investigation are 2,5-distyrylpyrazine (DSP), 1,4-bis (β-pyridyl-2 vinyl) benzene (P2VB), and 1,4 bis (2-methylstyryl) benzene (MSB) as efficient donors of intense absorption in the UV-region. AgNPs enhance the rate of energy transfer from DOLDs to TPPS via bringing donor and acceptor into close- proximity with a concomitant increase in dipole–dipole interaction between excited state donor and ground-state acceptor. The DOLDs molecular structures were optimized using the DFT/CAM-B3LYP/6-311G ++ (d, p) level of theory. The calculated electronic absorption spectra for the studied DOLDs

* Corresponding author at: Chemistry Department, Faculty of Science, Tanta University, Tanta, Egypt.
E-mail address: s.alhazmy@qu.edu.sa (E.-Z.M. Ebeid).
Peer review under responsibility of King Saud University.

Production and hosting by Elsevier

https://doi.org/10.1016/j.jscs.2022.101491
1319-6103 © 2022 The Author(s). Published by Elsevier B.V. on behalf of King Saud University.
This is an open access article under the CC BY license (http://creativecommons.org/licenses/by/4.0/).

in the gaseous phase and methanol solvent were studied using the time-dependent density functional theory (TD-DFT) at M06-2X/6-311G + + (2d,2p) level. The calculated absorption/emission spectra for DSP laser dye in methanol are obtained at the TD/ M06-2X/6-311G + +(2d, 2p) method. Notably, all theoretical results of the molecular structures under study highly agreed with the practical optical results. Energy transfer rate constants (k_{ET}) amid energy donor/acceptor pairs were determined by Stern-Volmer constants (KSV) and donors' lifetime measurements. The KSV values indicate an enhanced Fluorescence Resonance Energy Transfer (FRET) efficiencies in the presence of negatively charged AgNPs. The critical transfer distances R_o were determined from the spectral overlap between the emission spectrum of donor and absorption spectrum of TTPS. These outcomes propose the application of designed metal-enhanced FRET for energy-transfer-based assays and photodynamic therapy (PDT) applications.

© 2022 The Author(s). Published by Elsevier B.V. on behalf of King Saud University. This is an open access article under the CC BY license (http://creativecommons.org/licenses/by/4.0/).

1. Introduction

Porphyrin compounds have emerged in various applications, including nonlinear photonic devices, optical limiters, and optical switches, due to their unique optical properties [1–4]. Metalloporphyrins and water-soluble porphyrins were demonstrated as antibacterial and anti-HIV agents. Furthermore, they were used in singlet oxygen imaging and photosensitization [5,6]. One of the most crucial water-soluble porphyrin derivatives is the synthetic meso-tetrakis (4-sulfonatophenyl) porphyrin (TPPS) [7]. TPPS was evaluated and manipulated in clinical trials as an encouraging sensitizer for PDT [8]. Besides, TPPS has nonlinear optical absorption [9], which can prompt its application in photonic gadgets like optical limiters [10] and aggregation properties utilizing singlet oxygen production [11]. Furthermore, previous reports investigated the absorbance changes and static quenching of TPPS fluorescence by trinitrotoluene (TNT) to study the ground state interactions [12].

The interaction between TPPS in an excited state with different colloidal nanoparticles such as TiO_2 nanoparticles [13] and CdS quantum dots (QDs) [14] was investigated. It was found that the TPPS was anchored on both colloidal semiconducting nanomaterials (TiO_2 and CdS) surface through the sulphite (SO^{3-}) group as an anchoring group [13,14]. It was found that the TPPS could take an interest in the extinguishing system by infusing electrons from its excited states into the conduction band in nano TiO_2. Likewise, Renganathan studied the photoinduced interaction of water-soluble negatively charged thioglycolic acid (TGA) capped CdTe QDs as a donor with three porphyrin derivatives having different charges as accepters. Negatively charged TPPS revealed a Fluorescence Resonance Energy Transfer (FRET) mechanism, while positively charged meso-tetra (4-N-methyl pyridyl) porphyrin (TMPyP) displayed a charge/electron transfer mechanism [15,16].

Diolefinic compounds are catchy molecules because they are highly fluorescent materials with various applications such as laser dyes, electrochromic displays, optical imaging devices, and UV stabilizers of polymers [17,18]. Within this family, blue-emitting 1,4-bis (β-pyridyl-2 vinyl) benzene (P2VB), 2,5 distyrylpyrazine (DSP), and 1,4-Bis(2-methylstyryl)benzene (MSB) are important candidates in laser applications. For their significant applications, many studies have investigated their behavior as fluorescence energy donors [19]. For instance, energy is transferred from DSP and P2VB as donors to Rhodamine 110 in various solvents [20]. The experimental calculations of the critical distance indicated that the energy transfer was of Förster type [20]. On the other hand, MSB fluorescence photo-physically interacted with CCl_4 and aniline revealing a combined static and dynamic fluorescence quenching [21].

Recently, the interaction between fluorophores and metallic nanoparticles has been considered as a key feature of nanotechnology research due to their wide variety of applications [22,23]. The enhancement in the fluorescence efficiency in the presence of metallic nanoparticles is attributed to the strong coupling between the electronic transition dipole moment of the fluorophore with surface plasmon in metallic nanoparticles [24]. On the contrary, metallic nanoparticles act as quenchers when they interact with some organic fluorophores, and it was thought to arise from dynamic quenching [25]. Other researches revealed mixed static and dynamic types associated with the nano-quenchers systems [26]. The past theoretical studies recommended the presence of metal nanoparticles to boost the strength of the Donor/Acceptor (D / A) interactions and therefore, increase the efficiency of FRET between D and A in the vicinity of the metal particle [24,27].

The impact of metallic silver nanoparticles (Ag NPs) on FRET between a close D/A pair is best probed by measuring fluorescence in both collected and single-atom fluorescence identifications [28]. These earlier studies revealed that the emission intensities and lifetimes demonstrated that the enhancement in FRET efficiency was due to the metallic nanoparticles. The presence of metallic nanoparticles led to an increase in the Förster distance (R_o) for energy transfer from 8.3 to 13 nm. The rate constant of FRET was multiple times faster in the presence of Ag NPs than in the unbound donor/acceptor pairs [29]. This type of enhancement was attributed to the strong electromagnetic field surrounding metallic nanoparticles, which improved long-range dipole–dipole interaction that increased the final nonradiative resonance energy transfer. Since FRET results from the weak electromagnetic coupling of two dipoles, the introduction of additional dipoles found in metallic NPs can provide much more coupling interactions [29]. Up to our knowledge, till now, there are only a modest number of reports discussing the modification of energy transfer by the presence of plasmonic nanoparticles.

Herein, we study critical interactions of three diolefinic dyes DOLDs (DSP, P2VB, and MSB) as donors with a negatively

charged TPPS as an accepter to unveil the role of molecular charge on the energy transfer efficiency. Besides, this study reveals the enhancement of the FRET through the presence of metallic Ag NPs. The current outcomes recommend the utilization of metal-upgraded FRET for estimating the length of enormous biomolecules or for FRET-based assays and metal-enhanced fluor-immunoassay [24,29,30].

The themes and the novelty of this manuscript include the following: (1) effect of negatively charged Ag NPs on the FRET from DOLDs to TPPS and proposed a mechanism to be a kind of nano-immobilization DOLDs to enhance the interaction with TPPS in the medium of the study, (2) Spectroscopic investigations of both ground and excited states of the dyes under study, (3) photophysical interactions between DOLDs and TPPS, and (5) compare theoretical results obtained using DFT and TD-DFT calculations with experimental results.

2. Experimental

2.1. Materials

DSP and P2VB were prepared by the method described by Hasegawa et al. [31] Extensive purifications were achieved by column chromatography on silica gel using methylene chloride as eluent. The chromatographed material was then vacuum sublimed in the dark. The citrate reduction method of $AgNO_3$ was employed to get silver nanoparticles (Ag NPS) [32]. A typical solution of 60–80 nm diameter Ag NPs exhibiting a characteristic surface plasmon band around 420 nm was obtained. Citrate trisodium salt (95%, $C_6H_5O_7Na_3{\cdot}2H_2O$) was purchased from *Fluka*. MSB, Sodium salt of meso-tetrakis (4-sulfonatophenyl) porphyrin" (TPPS), and silver nitrate ($AgNO_3$) were acquired from *Sigma-Aldrich*.

2.2. Synthesis of Ag NPs

Ag NPs were prepared by applying the citrate reduction of $AgNO_3$ [32]. An aqueous solution of $AgNO_3$ (1 mM, 125 ml) was heated until it started to boil, then 5 ml of 1% trisodium citrate solution (as nucleating and reducing agent) was added quickly, which resulted in a change in solution color to pale yellow. After the color changed, the solution was removed from the heating element and allowed to stir until cool to room temperature. A typical solution of silver nanoparticles exhibiting a characteristic surface plasmon band around 420 nm was obtained [32]. For 10 nm diameter Ag NPs, the extinction coefficient was calculated as $1.328 \times 10^7\ M^{-1}\ cm^{-1}$, which compares with the literature value [32].

The prepared Ag NPs were characterized by electronic absorption spectroscopy and by Transmission Electron Microscopy (TEM).

2.3. Spectroscopic measurements and nanoparticle characterizations

The electronic absorption spectra were recorded utilizing the Shimadzu UV-3101 PC spectrophotometer. The steady-state fluorescence spectra were recorded employing the Perkin-Elmer LS-50B scanning Spectrofluorometer, using matched quartz cuvettes. The nanoparticle size was characterized by a transmission electron microscope (TEM), JEOL JEM-100SX Electron Microscope with a field gun, and an accelerating voltage of 80 kV.

2.4. DFT and TD-DFT calculations

All geometry optimizations of the compounds were executed using the DFT method implemented in Gaussian 09 program. Further, the calculated electronic absorption spectra for the studied DOLDs molecular structures in gas and methanol solvents were done via utilizing time-dependent density functional theory (TD-DFT) at M06-2X/6-311G++ (2d, 2p) level. Molecular electrostatic potentials (MESP) of DOLDs and TPPS were calculated at the B3LYP/6-311++G (d, p) level of theory in the gas phase. The hyperconjugation interactions in DSP molecular structure were examined via NBO analysis theory utilizing B3LYP/6-311G++(d, p)) level of theory.

3. Results and discussion:

3.1. Electronic absorption and emission spectra of DOLDs (Experimental Spectra)

Fig. 1 shows the electronic absorption and emission spectra of DOLDs and TPPS. The absorption spectra of 1×10^{-5} M DOLDs methanolic solutions revealed broad peaks with absorption maxima at 379, 353, and 344 nm for DSP, P2VB, and MSB, respectively. These peaks are ascribed to the extended π-network with π-π* and n-π* transitions [19,21]. Emission spectra of DSP show a broad emission peak with maximum at 447 nm and FWHM of 60 nm, while P2VB and MSB show a nearly split peaks at 397 nm and ~ 416 nm, which might be due to the specific solvent effect. These dyes have a characteristic high quantum yield, making them potential candidates in laser applications [19,21]. The calculated Fluorescence Quantum Yields (FQY) were 0.35, 0.46, and 0.7 for DSP, P2VB, and MSB, respectively.

3.2. Fluorescence quenching study of DOLDs

Fig. 2a, b, and c depects the effect of the sequential addition of TPPS (as an energy accepter) on the emission spectra of DOLDs (DSP, P2VB, and MSB) as energy donors. A remarkable fluorescence quenching was observed with increasing TPPS concentrations. Fig. 2d displays the Stern–Volmer plots (derived from Eqs. (2) and (3)) of DOLDs fluorescence quenching using TPPS as a quencher or an accepter [28].

$$\frac{I_o}{I_f} = 1 + K_{sv}\ [TPPS] \tag{2}$$

$$\frac{I_o}{I_f} = 1 + K_{ET}\ \tau_f\ [TPPS] \tag{3}$$

Where I_o and I_f are the fluorescence intensities in the absence and presence of the quencher TPPS. The Stern-Vomer constants (K_{SV}) were calculated as $4.45 \times 10^4\ M^{-1}$, $1.86 \times 10^4\ M^{-1}$, and $1.89 \times 10^5\ M^{-1}$ for DSP, P2VB and MSB, respectively. These values demonstrate the physical interaction of the dyes with TPPS rather than the spectral

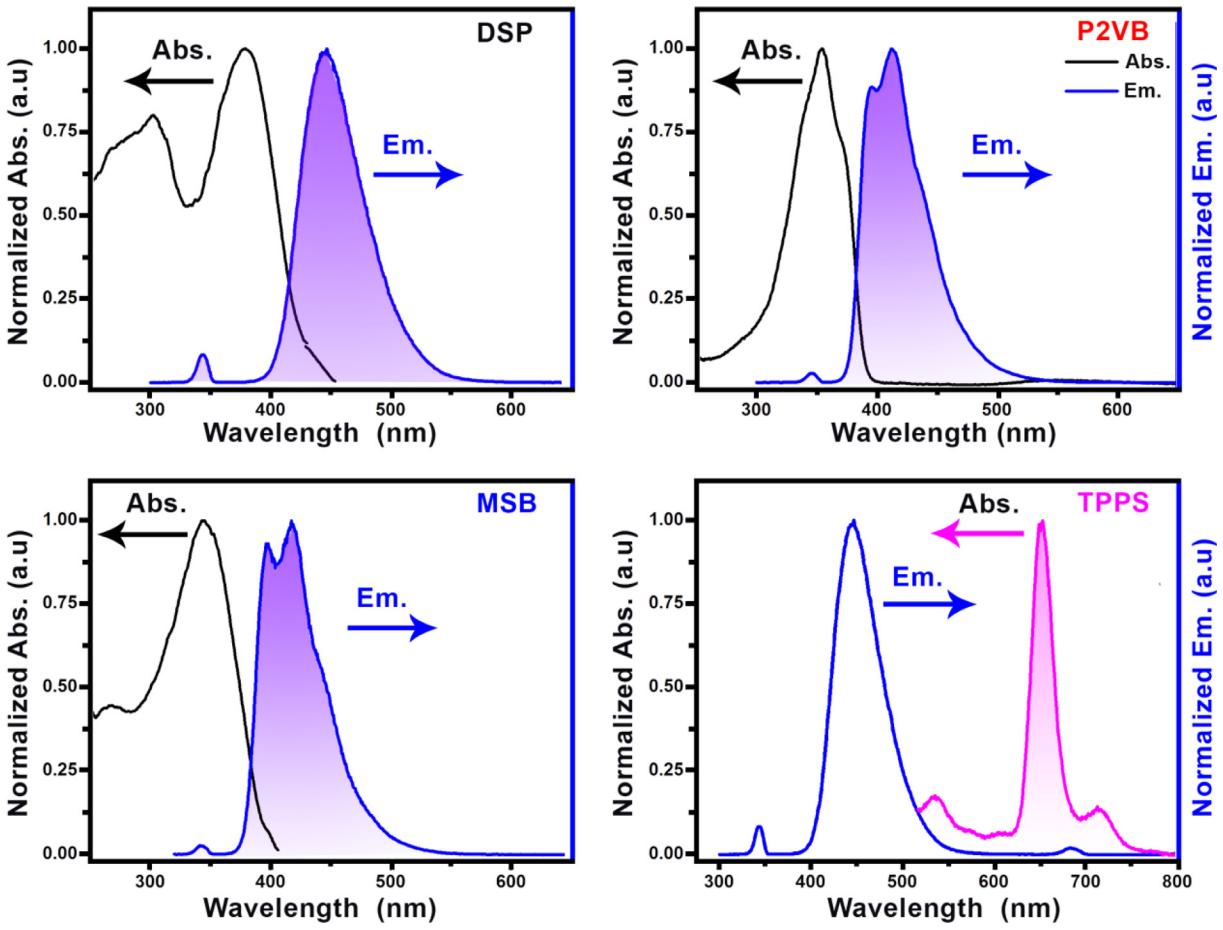

Fig. 1 Experimental absorption and emission spectra for 1×10^{-5} M methanolic solutions of DOLDs (DSP, P2VB and MSB) and TPPS.

overlap that follows a different series, as shown in Fig. 2f. The rate constants of energy transfer (k_{ET}) were calculated, taking the lifetime as τ_o = 1.44 ns, 0.42 ns, and 1.63 ns for DSP, P2VB, and MSB, respectively, in methanol [19,20], and were found to be $k_{ET} = 0.31 \times 10^{14}$ $M^{-1}s^{-1}$; 44.00×10^{14} $M^{-1}s^{-1}$, and 1.33×10^{14} $M^{-1}s^{-1}$ for DSP, P2VB and MSB, correspondingly. The significantly elevated value in the case of P2VB/TPPS indicates the high fast time-domain quenching process of TPPS to P2VB, which has the shortest excited state lifetime. The current values of the rate constants of energy transfer for the current DOLDs are much higher than the diffusion rate constant in methanol ($k_d = 1.8 \times 10^9$ $M^{-1}s^{-1}$) at room temperature, indicating a long-range energy transfer mechanism of dipole–dipole interaction between the excited state of DOLDs and ground state TPPS [24,27].

The mechanism of fluorescence quenching of DOLDs by TPPS as an energy accepter was investigated in a higher viscosity medium containing 40% ethylene glycol by volume at room temperature. As the concentration of the TPPS increases, the fluorescence intensities of DOLDs decrease without a change in spectral pattern, referring to the absence of excited state complex formation (Exciplex). Besides, this enhancement in energy transfer constant by increasing viscosity is consistent with the diffusionless energy transfer mechanism [24]. Meanwhile, this increase in the k_{ET} and K_{SV} values indicates a static quenching mechanism and solvent cage effect [19]. The value of critical energy transfer distance (R_o), to be discussed later in detail, manifested a small space between DOLDs and TPPS due to the cage effect upon increasing medium viscosity.

The Perrin model was applied for the energy transfer according to the following equations: [33]

$$ln \frac{I_o}{I_f} = \mathbf{V} N_o [Q] \tag{4}$$

$$\mathbf{V} = \frac{4}{3}\pi \mathbf{r}^3$$

where I_o and I_f are emission intensities in the absence and presence of a quencher, V is the volume of the quenching sphere in cubic centimeters, N_o is the Avogadro's number, and [Q] is the molar concentration of the quencher.

A plot of ln (I_o/I_f) versus [Q] demonstrated linear behavior in Fig. 2e, and the slopes equal VN_o. "V" values were found to be 4.23×10^{-16}, 2.04×10^{-16}, and 1.65×10^{-16} cm^3. The radius of quenching sphere "**r**" was calculated as 46.58, 36.53, and 73.36 nm in the case of DSP/TPPS, P2VB/TPPS, and MSB/TPPS, respectively. These low values of quenching radius emphasize a ground-state complex, which results in the current quenching of DOLDs by TPPS. When the TPPS molecules bind with the DOLDs, the equilibrium between

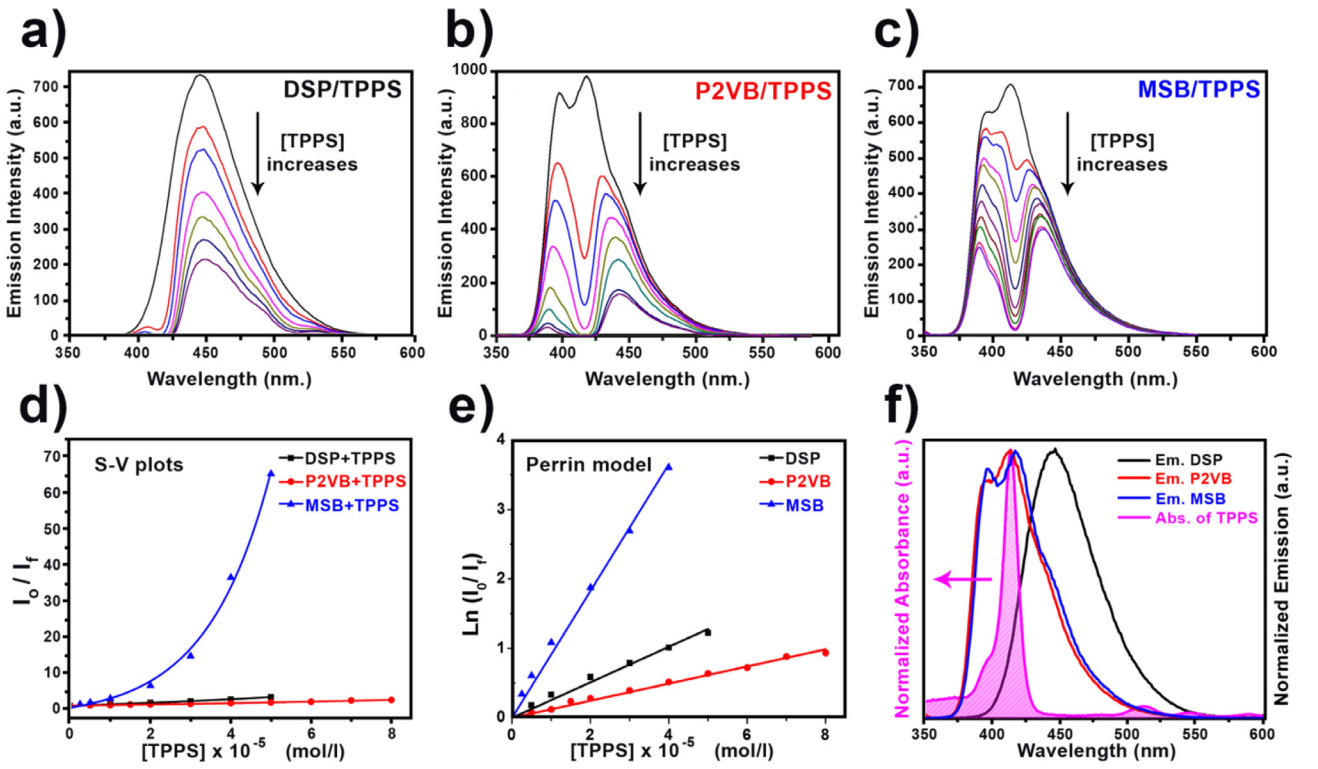

Fig. 2 Emission spectra of (a) DSP (b) P2VB (c) MSB at different TPPS of concentrations (d) Stern-Volmer plots, (e) Perrin model curves, and (f) Spectral overlap between DOLDs donor's emissions with TPPS accepter absorption.

the bound and free molecules can be treated in our systems according to Eq. (6) [34]

$$\boldsymbol{log}\left(\frac{\boldsymbol{I_o - I_f}}{\boldsymbol{I_f}}\right) = \mathbf{logK} + \mathbf{n}\log[\boldsymbol{TPPS}] \tag{6}$$

where "K" and "n" are the limiting steady and the quantity of restricting locales, individually. The upsides of n and K can be determined from the plot of $\boldsymbol{log}\left(\frac{I_o - I_f}{I_f}\right)$ versus log[*TPPS*] as in Fig. S1. The relating results are summarized in Table S1. The calculated binding sites were near unity because of the interaction between negatively charged SO^{3-} groups in TPPS and the partially positive terminals of DOLDs.

To deeply examine the FRET mechanism between the electronic ingestion range of TPPS and discharge range of DOLDs, as displayed in Fig. 2f, the basic exchange distance of the D / A pair was determined utilizing the Förster formulation (7,8):

$$\mathbf{R_o^6} = 8.79 \times 10^{-5}\left(\mathbf{k^2 n^{-4} \Phi_f J(\lambda)}\right)\mathbf{in^6} \tag{7}$$

where $\boldsymbol{R_o}$ is the Förster critical transfer distance at which 50% of the excitation energy is transferred to the accepter (50% transfer efficiency), ($\boldsymbol{n}$) is the refractive index of the solvent, ($\boldsymbol{k^2}$) = 2/3, (Φ_f) is the donor fluorescence quantum yield, and $\boldsymbol{J(\lambda)}$ is the "overlap integral", which expresses the extent of spectral overlap between the donor emission and acceptor absorption and is given by:

$$\mathbf{J}(\lambda) = \int_o^\infty \mathbf{F_D}(\lambda)\varepsilon_\mathbf{A}(\lambda)\lambda^4 \mathbf{d}\lambda \tag{8}$$

where $\varepsilon_A(\lambda)$ is in M^{-1} cm^{-1}, (λ) in nm and the unit of $\boldsymbol{J}(\boldsymbol{\lambda})$ is in M^{-1} cm^{-1} $(nm)^4$, $\boldsymbol{F_D}$ is the peak-normalized fluorescence spectrum for the donor, and (ε_A) is the molar absorption coefficient for the accepter. These values are higher than that for the collisional energy-transfer mechanism in which R_o should be less than 10 nm [35]. The high value of critical transfer distance and the energy-transfer rate constants indicate that the current energy transfer mechanisms in the investigated Donor/Acceptor (D/A) pairs are a resonance energy transfer due to long-range dipole–dipole interaction between the excited donor (D*) and the ground state accepter (A). This type of interaction is Förster Resonance Energy Transfer (FRET), which involves an electrostatic interaction between D (DOLDs) and A (TPPS). These interactions can occur over a long-range over D/A distances as 50–100 Å [36].

3.3. DFT calculations

The DOLDs (DSP, MSB, and P2VB) optimized structures of their electronic ground states were obtained employing the DFT method at CAM-B3LYP/6-311G + + (d, p) level of theory. Besides, all geometry optimizations of the compounds were performed using the DFT method implemented in Gaussian 09 [37]. The obtained optimized structures are shown in Fig. 3, in which DSP and P2VB molecular modeling structures are planar, but MSB is not planar. The important selected optimized structural parameters are summarized in Table S2, parameters such as (bond length (BL) in Å, bond angle (BA) in degrees (°), and dihedral angle (DA) in degrees (°) for DSP, MSB, and P2VB in the gas phase via applying DFT theory at CAM-B3LYP/6-311G + + (d, p) level. Significant comments can be deduced from Fig. 3 and Table S2, and they can be expressed as follows; (i) referring to the listed values of dihe-

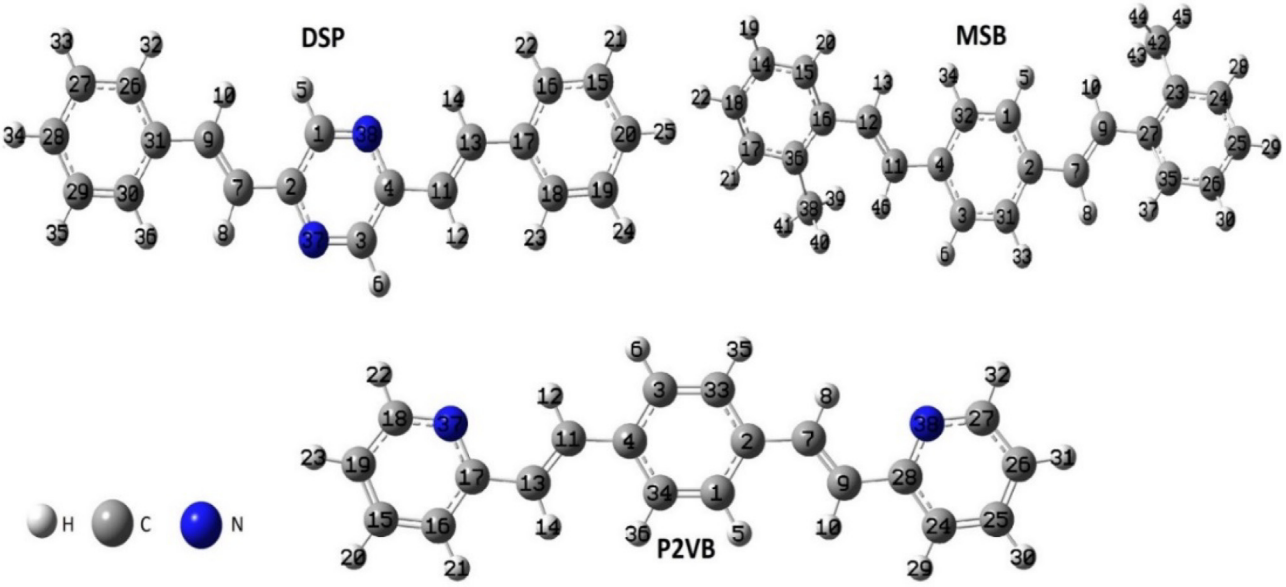

Fig. 3 Optimized molecular structures of DOLDs in gas state using CAM-B3LYP/6-311G + + (d, p) level of theory.

dral angles, the two styryl groups, and pyrazinyl of DSP molecular structure lie in the same plane. In P2VB laser dye, the two pyridyl groups lie in the same plane as the two vinyl and benzene groups. However, the two methyl benzene groups of MSB molecular structure rotate out of the two vinyl and benzene groups by an angle of 150°. (ii) owing to increasing bond order, the C_1–C_2 bond length is less than C_2–C_7 bond lengths in all DOLDs molecular structures by about 0.06 Å. (iii) referring to the listed values of bond angles, the type of hybridization over all DOLDs is sp^2.

Fig. 4 demonstrates the obtained results of all DOLDs molecular orbitals. (MOs) modeling of HOMO (H)/LUMO (L) orbitals, H−1/L+1, H−2/L+2, and energy gaps between the following graphically; H and L (E_{g1}), H−1 and L+1 (E_{g2}), and H−2 and L+2 (E_{g3}) in the gas state via utilizing CAM-B3LYP/6-311G + + (d, p) level of theory. The energy values of H (E_H), L (E_L), H−1 (E_{H-1}), L+1 (E_{L+1}), H−2 (E_{H-2}), and L+2 (E_{L+2}). Also, the energy gap (E_g) between H and L (E_{g1}), H−1 and L+1 (E_{g2}), and H−2 and L+2 (E_{g3}) in the gas state are listed in Table S3. Due to the conjugation in the molecular structures of the studied DOLDs, the HOMO and LUMO MOs are delocalized over the whole DOLDs molecular modeling structures. The energy gap (E_{g1}) value is calculated by applying the difference (E_H-E_L). The calculated E_{g1} values for DOLDs rise in the following order: MSB < DSP < P2VB. These results indicate that the MSB molecular modeling structure is more reactive than DSP and P2VB molecular structures.

Of Note, considerable chemical quantum parameters like dipole moment (**μ**), chemical potential (**ρ**), electronegativity (**χ**), and chemical hardness (**η**) were calculated using E_L and E_H values. These quantum parameters are calculated using equations $\rho = \frac{E_H+E_L}{2}$ [39], $\chi = -\frac{E_H+E_L}{2}$, and $\eta = \frac{E_L-E_H}{2}$ [38].

It is noteworthy that when a chemical structure has a high dipole moment, it has a significant asymmetry in the electronic charge distribution. It can be highly sensitive due to changes in chemical structure and electronic properties under an external electric field. Thus, as shown in Table S4, the **μ** value of the compound P2VB is high compared to the rest of the compounds under study, namely MSB and DSP, and therefore this compound is more active than the rest of the compounds under investigation. As presented in Table S4, the **ρ** value of MSB molecular structure is lower compared to the other DOLDs compounds, namely (P2VB and DSP). These results indicate that the escaping electrons from MSB molecular structure are less compared to other compounds under the current study. Of Note, the high **χ** value for MSB molecular structure compared to P2VB and DSP leads to this compound's ability to attract electrons from other compounds [39]. On the other side, the **η** value for MSB molecular structure's < UNK > value is high compared to the other compounds (P2VB and DSP) (listed in Table S4). These results show that MSB compound is undeniably challenging to free electrons, while the structures of P2VB and DSP are extraordinary chances to offer electrons to another acceptor molecule.

3.4. TD-DFT calculations

The calculated electronic absorption and emission spectrum for DSP laser dye in methanol are obtained via the TD/M06-2X/6-311G + + (2d, 2p) method. The results are presented in Fig. 5a. Fig. 5b, and display the calculated electronic absorption spectra for the studied MSB and P2VB molecular structures in gas and methanol solvent. These calculations were done by utilizing time-dependent density functional theory (TD-DFT) at M06-2X/6-311G + + (2d, 2p) level.

It is significant to discuss the following notes for a clear comparison between theoretical and experimental results. The experimental absorption spectra of DOLDs in methanol revealed a broad peak with absorption maxima (λ_{exp}) of 379 nm, 353 nm, and 344 nm for DSP, P2VB, and MSB, respectively as shown in Fig. 1. These peaks are attributed to the extended π-network with π-π* and n-π* transitions. The maximum calculated electronic absorption spectra (λ_{calc}) and

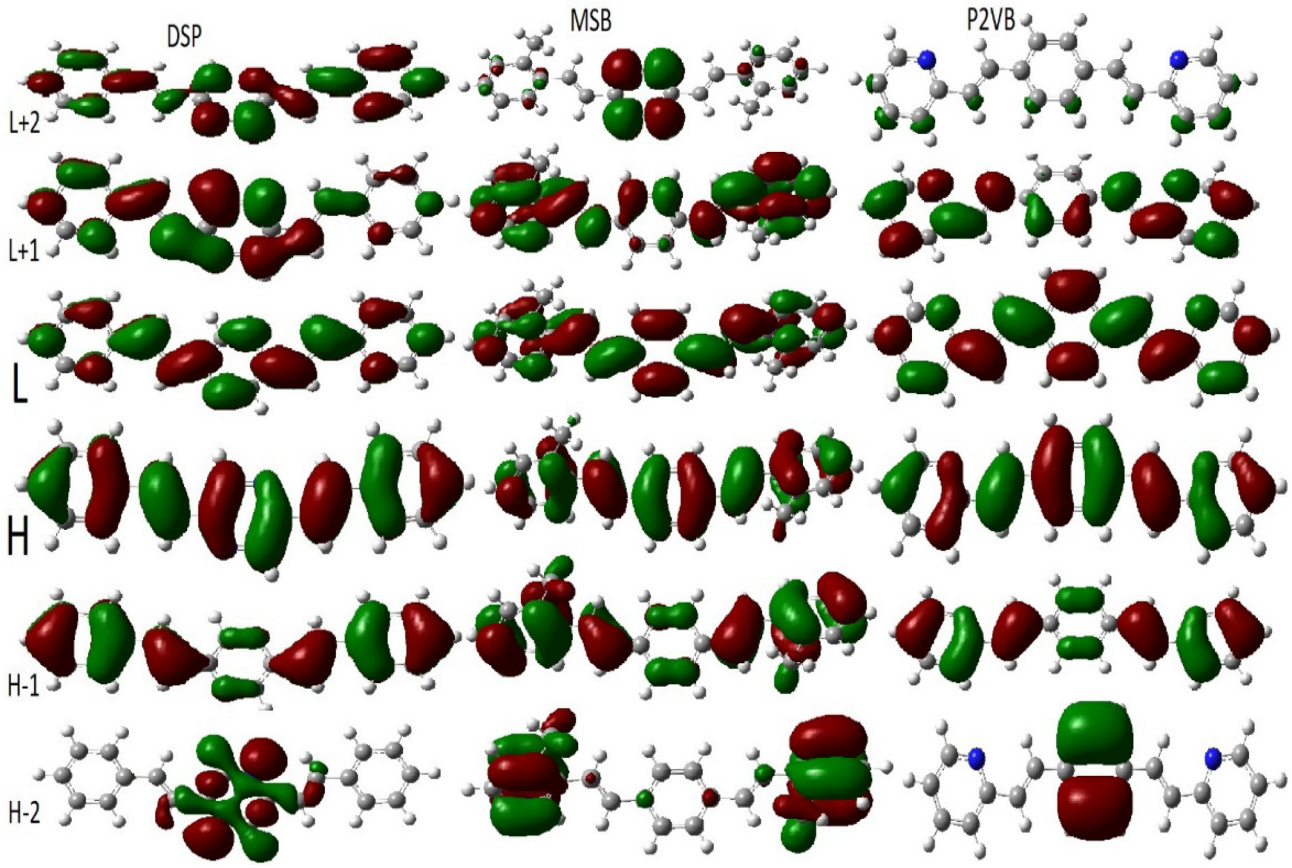

Fig. 4 DOLDs (DSP, MSB and P2VB) molecular modelling graphical presentation of HOMO (H) / LUMO (L) orbitals, H−1/L + 1, H−2/L + 2 in gas state via utilizing CAM-B3LYP/6-311G + + (d, p) level of theory.

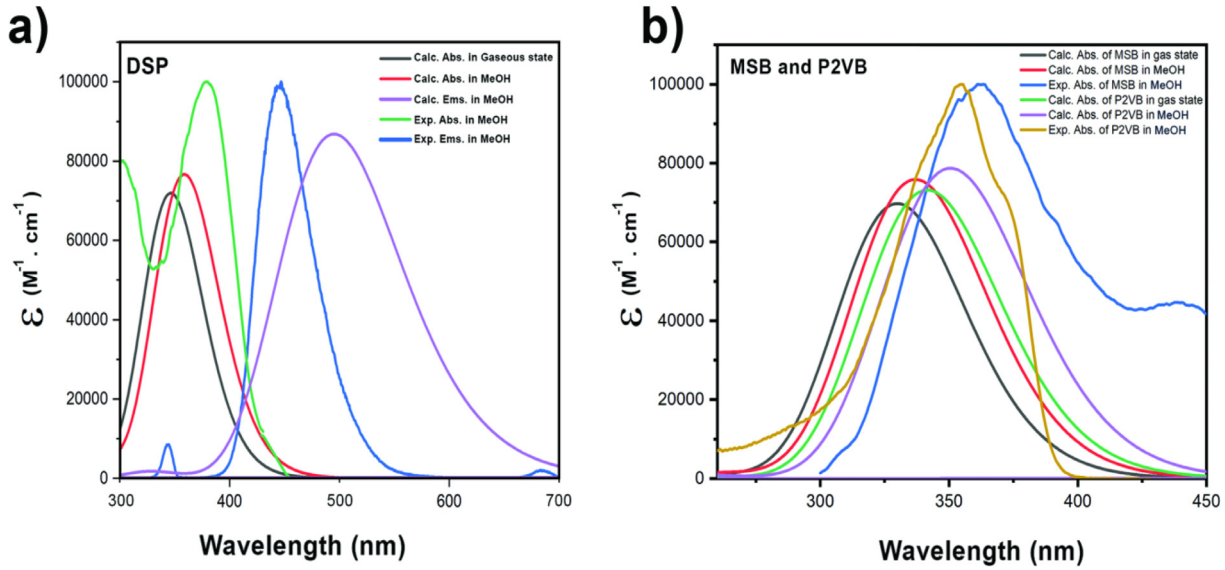

Fig. 5 (a) Calculated (Calc.) and experimental (Exp.) absorption (Abs.) and emission (Ems.) spectra of DSP molecular structure in gas and methanol. (b) The calculated absorption spectra of MSB and P2VB molecular structures in gas and methanol. The theoretical results are obtained using TD-DFT at M06-2X/6-311G + + (2d, 2p) level of theory.

oscillator strength for DSP, P2VB, and MSB molecular structures in methanol are (359 nm, 1.891), (351 nm, 1.943), and (336 nm, 1.872) respectively, as listed in Table S5. These results are attributed to π-π* and n-π* electronic transitions. Therefore, the difference between λ_{exp} and λ_{calc} for DSP, P2VB, and MSB molecular structures in methanol is 20, 2, and

8 nm, respectively. The maximum experimental and calculated emission wavelengths for DSP in methanol are 447 nm and 395 nm, respectively, as shown in Fig. 5a. Hence, the theoretical optical results of the molecular structures under study agree with the practical optical results. The calculated electronic parameters like excitation energy ($\mathbf{E_{exc.}}$), absorption maxima ($\boldsymbol{\lambda_{calc.}}$), electronic transition, and oscillator strength (f) for DOLDs molecular structures in methanol are obtained and listed in Table S5. The calculated electronic transition maxima for DSP, MSB, and P2VB molecular structures in methanol appear at one electronic transition at 358.73, 336.96, and 350.54 nm, respectively. These arise from electronic transition HOMOs to LUMOs, where the oscillator strength is in the range (f = 1.943–1.891), and the coefficient is 0.941, which highly agrees with the experimental results.

3.5. Molecular electrostatic surface potential (MESP) investigation

The molecular electrostatic interactions between DSP, P2VB, MSB, and TPPS, were examined via the Molecular Electrostatic Surface Potential (MESP) [40], as shown in (Fig. 6a and b). TPPS displays a significant negative electrostatic potential (V = ∼−176 kcal/mole) situated on the SO^{3-} group, where less negative charge is positioned on the porphyrin skeleton (V = ∼−151 kcal/mole). On the other hand, the DOLDs show the presence of terminal positive electrostatic potential 11.3, 6.1, and 11.9 for DSP, MSB, and P2VB, correspondingly. Upon addition of TPPS to the DOLDs, electrostatic attraction and sequential charge transfer stabilized the molecular complexes.

3.6. Natural bond orbital (NBO) analysis

Since resonance is a fundamental phenomenon in the stability of the organic chemical structure, it was essential to study the stability of the chemical structure using Natural Bond Orbital (NBO) analysis for one of the DOLDs under the current study as an example, and we chose the DSP molecule. The hyperconjugation interactions in DSP molecular structure are examined via NBO analysis theory utilizing B3LYP/6-311G + +(d, p)) level of theory [41]. Besides, these results were obtained by utilizing second request annoyance energies (E2) [41]. The utmost influential second-order perturbation (E2) delocalization energies in the DSP molecule in its gas phase are listed in Table S7. These are classified as π-π* and n-π* interactions, with the latter having larger energy magnitudes. The intense interaction between C_1-C_2 π-bond to C_3-N_{37} π-antibonding stabilized

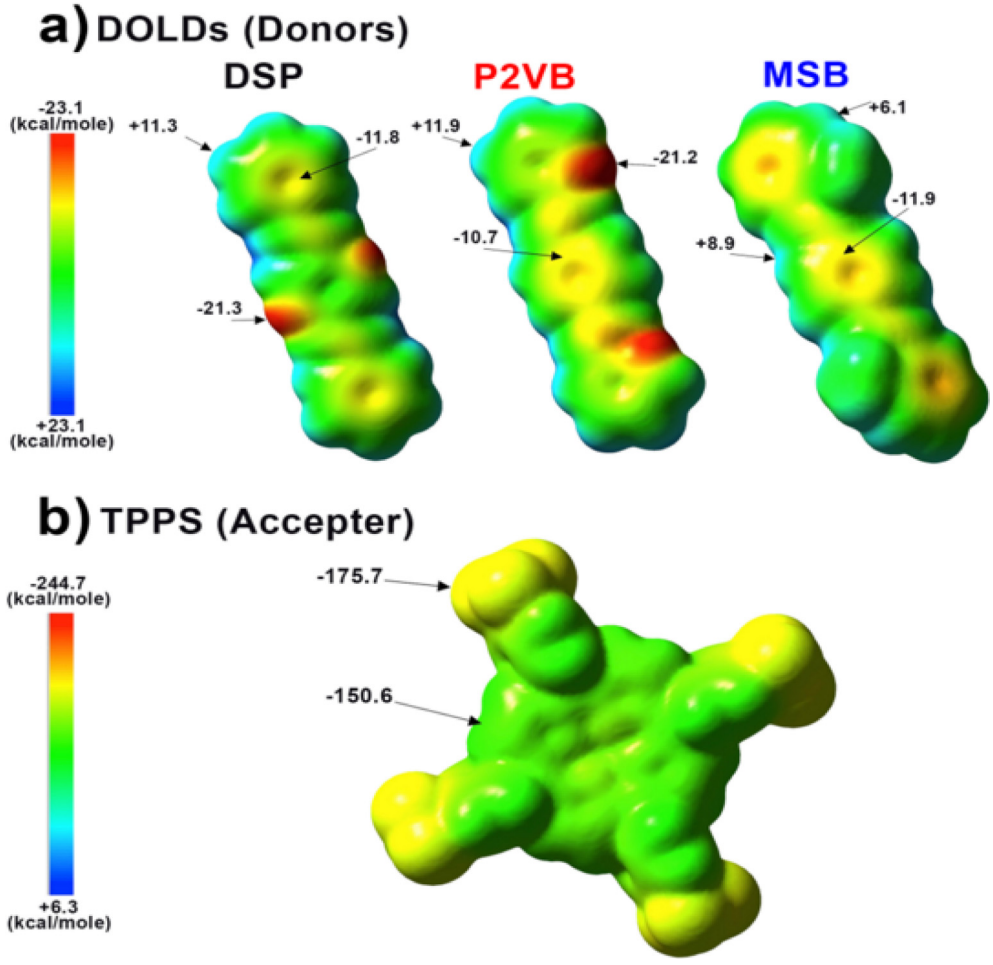

Fig. 6 (a) Molecular electrostatic potentials (MESP) of DOLDs and (b) TPPS, calculated at B3LYP/6–311 + + G (d, p) level of theory in the gas phase.

DSP molecular structure by 22.84 kcal/mol, then from C_3-N_{37} π-bond to C_4-N38 π-antibonding via 20.71 kcal/mol. Also, the interaction between C_{17}-C_{30} bond and C_{26}-C31 π-antibonding stabilized DSP molecule by 14.70 kcal/mol, then from C_{15}-C_{20} π-bond to (C16-C17 and C18-C19) π-antibonding that contributed 18.63 and 15.77 kcal/mol respectively as recorded in Table S7.

From the previous quantum calculations, the surface charge over DOLDs is positive, and hence introducing negatively charged silver nanoparticles (Ag NPs) would attach and immobilize the positively charged DOLDs. These immobilized DOLDs (Donors) on the Ag NPs surface are expected to improve the energy transfer to the available accepter in the medium (TPPS). So, under the current investigation, we designed an experiment in which negatively charged Ag NPs were involved in the medium to check its effect on the energy transfer between D/A pairs.

3.7. Enhancing the energy transfer from DOLDs to TPPS in the presence of Ag NPs:

Fig. 7a shows the TEM image of the prepared spherical Ag NPs, which have a diameter of around 30 nm and display their characteristic plasmonic absorption spectra around 425 nm (Fig. 7b). The fluorescence emission of DOLDs was studied with TPPS as an accepter in the presence of 20% Ag NPs in methanol and 40% ethylene glycol by volume at room temperature. As the concentration of the TPPS increases, the fluorescence intensities of DOLDs decrease. The K_{SV} constant of the process in the presence of Ag NPS is higher than that in the absence of Ag NPs (Fig. 7c–e). For instance, the K_{SV} value of the process in the presence of Ag NPs for DSP was $K_{SV} = 0.562 \times 10^5\ M^{-1} > K_{SV} = 0.447 \times 10^5\ M^{-1}$ in the absence of Ag NPs. These results could be accredited to the negative citrate capping groups on Ag NPs having a role in increasing the dipole–dipole (D/A) interactions via immobilizing the unbound D molecules [42].

Besides, the K_{SV} constant of the process in ethylene glycol (vol 40%) with Ag NPs (20 vol%) is less than that in methanol, as shown in Fig. 7(c, d, and e). These results may be interpreted as the role of the medium viscosity in decreasing the diffusion of both donor and accepter towards Ag NPs surface with a subsequent decrease in D/A interactions. On the other hand, considering the strong plasmonic nature of Ag NPs, and based on the spectral overlap contribution of Ag NPs to additively deactivate the excited state of DOLDs side to side with TPPS, Ag NPs can participate in the current quenching mechanism rather than being only as an immobilizing surface. Besides, since FRET results from the weak electromagnetic coupling of two dipoles, the introduction of additional dipoles found in Ag NPs can provide much more coupling interactions.

The proposed scheme of Ag NPs interaction with DOLDs/TPPS is graphically sketched in Fig. 8. Based on earlier

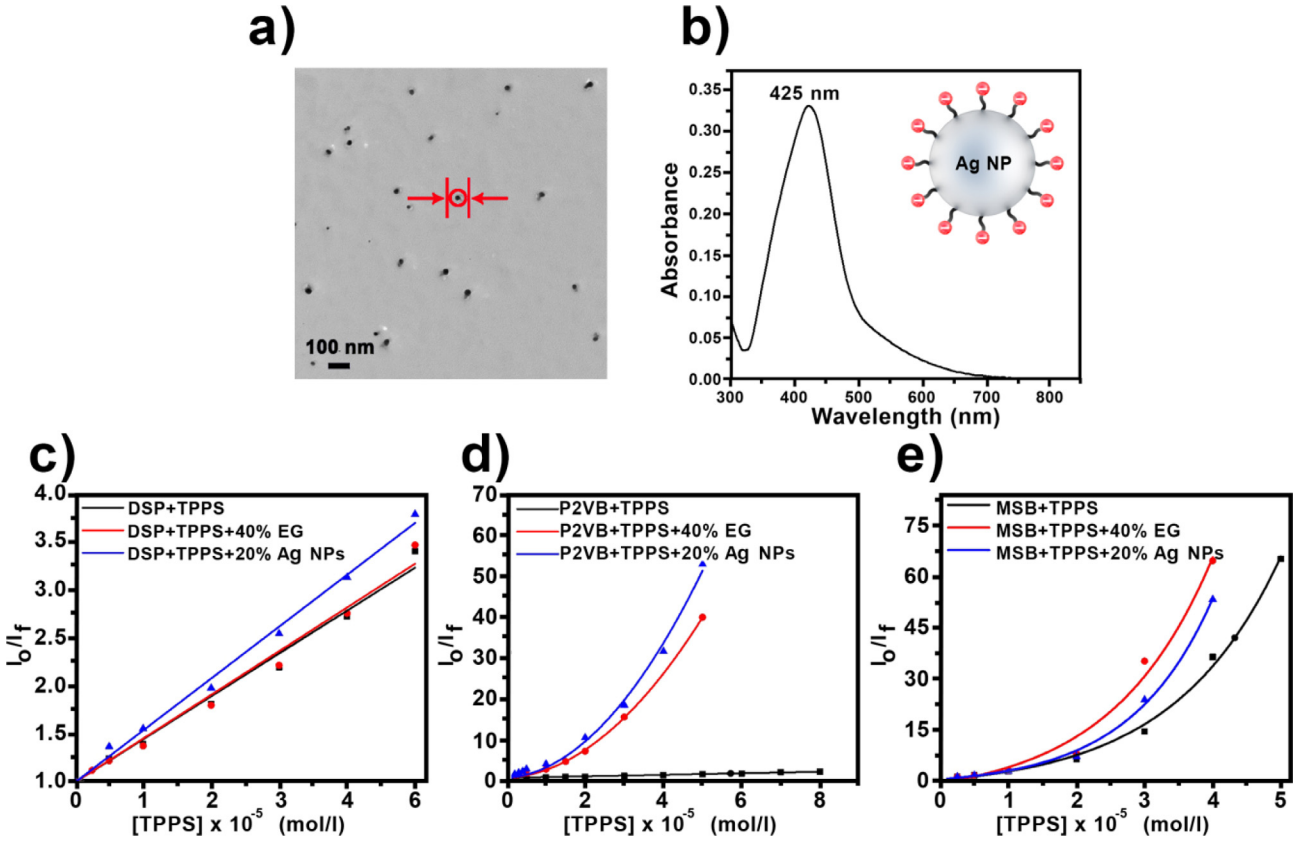

Fig. 7 (a) TEM micrograph of silver nanoparticles (Ag NPs), (b) Absorption spectrum of Ag NPs aqueous solution, Stern-Volmer plots of the quenching of 1×10^{-5} M (c) DSB (d) P2VB (e) MSB by TPPS in methanol, 40% ethylene glycol (EG) by volume in methanol and in presence of 20% Ag NPs in (water/methanol) by volume.

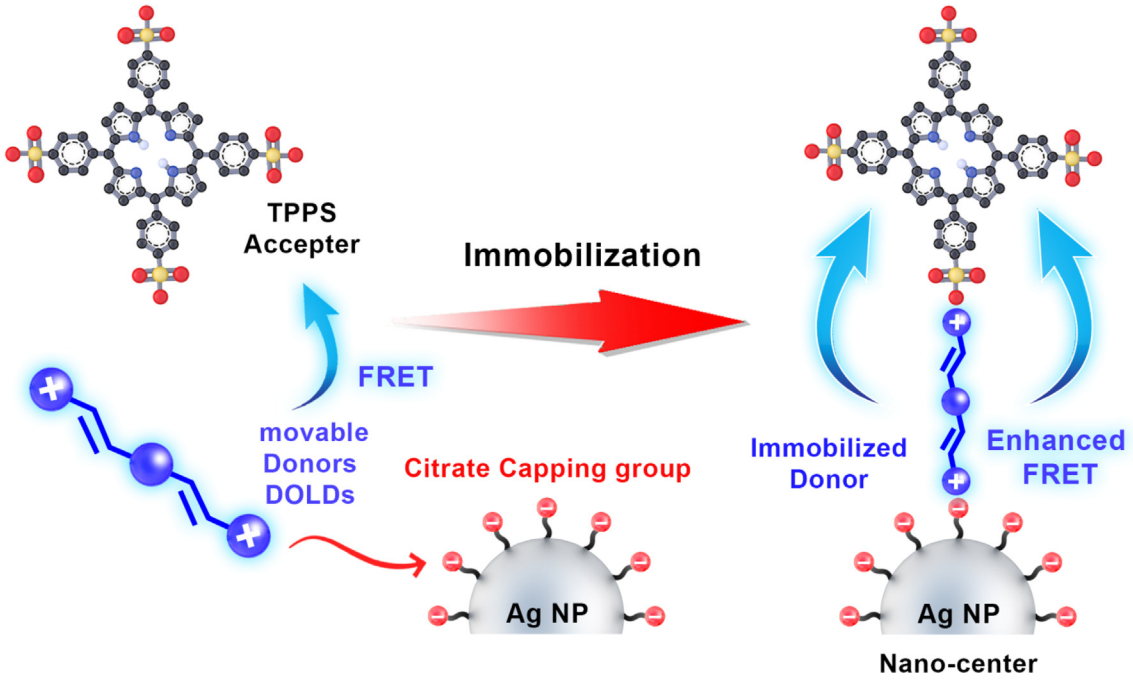

Fig. 8 Graphical illustration of the proposed effect of Ag NPs on the interaction between DOLDs and TPPS.

reports, it is proposed that negatively charged citrate-capped Ag NPs electrostatically attract the partially positively charged terminal of DOLDs on the nanoparticle surface [43]. The other side of DOLDs becomes free for transferring energy to TPPS more efficiently than the free DOLDs. This hypothesis of DOLDs / NPs interaction was previously reported by our group [44], in which the same DOLDs were used to induce the aggregation of citrate-capped gold nanoparticles (Au NPs) via the electrostatic interaction with the partially positive terminals in DOLD molecules. However, in our current study, the sequence of addition and the amount of Ag NPs (only 20 vol%) was not enough to cause noticeable aggregation of nanoparticles. Here, DOLDs were electrostatically attracted to the negatively charged Ag NPs, which causes donors' immobilization and increases the opportunity of FRET to TPPS. All emission spectra of DOLDs were recorded after the addition of Ag NPs and after the gradual addition of TPPS dye. Thus, the immobilization of D/A couples on the surface of Ag NPs increases the coupling exchange and dipole interaction between DOLDs and TPPS. The role of nanoparticles in enhancing FRET was reported for other systems [45,46].

4. Conclusion

In summary, this research aimed to unveil the photophysical interaction and Fluorescence Resonance Energy Transfer (FRET) from three DOLDs dyes as donors to TPPS as an acceptor via spectroscopic and theoretical studies. Besides, investigating the effect of Ag NPs presence on the FRET. Based on the spectral overlap and the molecular electrostatic potentials, the energy transfer between D-A pairs was long-range Förster Resonance Energy transfer type (R_o > 10 nm), which involves an electrostatic interaction between D and A accompanied by coupling between the two dipoles. The spectral study and DFT calculation for the current system revealed that the energy transfer was drastically affected by the donor's chemical structure, binding, electrostatic potential, and alignment to the acceptor. MSB has an energy transfer constant KSV four and ten times higher than DSP and P2VB. The addition of Ag NPs to these interacting constituents enhances the energy transfer via enhancing coupling exchange by immobilization of D-A pairs on Ag NPs' surface. These outcomes underscore the utilization of metal-improved FRET for estimating the closeness of huge biomolecules, energy-move-based examines, and photodynamic treatment applications. The calculated optical properties for DOLDs are obtained by utilizing time-dependent density functional theory (TD-DFT) at M06-2X/6-311G++ (2d, 2p) level. The calculated electronic transition for DSP, MSB, and P2VB molecular structures in methanol solvent appears at one electronic transition at 358.73, 336.96, and 350.54 nm, respectively. This arises from the electronic transition from HOMOs to LUMOs, where the oscillator strength is in the range (f = 1.943–1.891) and the coefficient is 0.941, which agrees with the experimental results. Furthermore, negatively charged Ag NPs led to immobilization of the positively charged DOLDs donors and, consequently, increased the opportunity for more FRET to TPPS acceptors in the medium. This study paves the way to apply metallic nanoparticle-enhanced FRET for biological assays, photodynamic therapy (PDT), and related biosensors.

Declaration of Competing Interest

The authors declare that they have no known competing financial interests or personal relationships that could have appeared to influence the work reported in this paper.

Acknowledgement

The authors like to thank the deanship of scientific research, Qassim University for funding the publication of this article.

References

[1] T. Ono, D. Koga, K. Yoza, Y. Hisaeda, The first synthesis of meso-dicycloalkylporphycenes: ring strain effects on structural and optical properties of isomeric porphyrins, Chem. Comm. 53 (91) (2017) 12258–12261.

[2] Y. Xu, Z. Liu, X. Zhang, Y. Wang, J. Tian, Y. Huang, Y. Ma, X. Zhang, Y.A. Chen, A graphene hybrid material covalently functionalized with porphyrin: synthesis and optical limiting property, Adv. Mater. 21 (12) (2009) 1275–1279.

[3] M.O. Senge, M. Fazekas, E.G.A. Notaras, W.J. Blau, M. Zawadzka, O.B. Locos, E.M. Ni Mhuircheartaigh, Nonlinear optical properties of porphyrins, Adv. Mater. 19 (2007) 2737–2774.

[4] J. Rong, N. Cecil, M. Magdaong, M. Taniguchi, J.R. Diers, D. M. Niedzwiedzki, C. Kirmaier, J.S. Lindsey, D.F. Bocian, D. Holten, Electronic structure and excited-state dynamics of rylene-tetrapyrrole panchromatic absorbers, J. Phys. Chem. A 125 (36) (2021) 7900–7919.

[5] J. Schmitt, V. Heitz, A. Sour, F. Bolze, H. Ftouni, J.-F. Nicoud, L. Flamigni, B. Ventura, Diketopyrrolopyrrole-porphyrin conjugates with high two-photon absorption and singlet oxygen generation for two-photon photodynamic therapy, Angew Chem. 127 (1) (2015) 171–175.

[6] E.I. Zenkevich, E.I. Sagun, V.N. Knyukshto, A.S. Stasheuski, V.A. Galievsky, A.P. Stupak, T. Blaudeck, C. von Borczyskowski, Quantitative analysis of singlet oxygen ($^1O_2$) generation via energy transfer in nanocomposites based on semiconductor quantum dots and porphyrin ligands, J. Phys. Chem. C 115 (44) (2011) 21535–21545.

[7] L. Liu, W. Jin, L. Xi, Z. Dong, Spectroscopic investigation on the effect of pairing anions in imidazolium-based ionic liquids on the J-aggregation of meso-tetrakis-(4-sulfonatophenyl) porphyrin in aqueous solution, J. Lumin. 131 (11) (2011) 2347–2351.

[8] L. Xia, J. Wu, B. Huang, Y. Gao, J. Tian, W. Zhang, Enhanced photodynamic therapy through supramolecular photosensitizers with an adamantyl-functionalized porphyrin and a cyclodextrin dimer, Chem. Comm. 56 (75) (2020) 11134–11137.

[9] D.J. Li, Z.G. Gu, J. Zhang, Auto-controlled fabrication of a metal-porphyrin framework thin film with tunable optical limiting effects, Chem. Sci. 11 (7) (2020) 1935–1942.

[10] T. Bai, N. Dong, H. Cheng, Q. Cheng, J. Wang, Y. Chen, $CH_3NH_3PbI_3$ perovskite: Poly (N-vinylcarbazole) blends for broadband optical limiting, RSC Adv. 7 (4) (2017) 1809–1813.

[11] G.G. Parra, D.S. Correa, J.E. Silveira-Alves, L.M. Almeida, M. A. Souza, L. De Boni, L. Misoguti, C.R. Mendonça, S.C. Zílio, N.M. Neto, I.E. Borissevitch, Effects of meso-tetrakis (4-sulfonatophenyl) porphyrin ($TPPS_4$) aggregation on its spectral and kinetic characteristics and singlet oxygen production, Spectrochim. Acta Part A Mol. Biomol. Spectrosc. 10 (2021) 120063–120070.

[12] M. Rahman, H.J. Harmon, Absorbance change and static quenching of fluorescence of meso-tetra (4-sulfonatophenyl) porphyrin (TPPS) by trinitrotoluene (TNT), Spectrochim. Acta Part A Mol. Biomol. Spectrosc. 65 (3-4) (2006) 901–906.

[13] A. Kathiravan, R. Renganathan, Effect of anchoring group on the photosensitization of colloidal TiO_2 nanoparticles with porphyrins, J. Colloid Interface Sci. 331 (2) (2009) 401–407.

[14] M. Asha Jhonsi, A. Kathiravan, R. Renganathan, An investigation on fluorescence quenching of certain porphyrins by colloidal CdS, J. Lumin. 129 (8) (2009) 854–860.

[15] M.A. Jhonsi, R. Renganathan, Investigations on the photoinduced interaction of water soluble thioglycolic acid (TGA) capped CdTe quantum dots with certain porphyrins, J. Colloid Interface Sci. 344 (2) (2010) 596–602.

[16] K. Velappan, R. Rajalingam, A. Venkattappan, Photoinduced electron transfer reactions of water soluble porphyrins in zeolite environment, J. Fluoresc. 31 (5) (2021) 1575–1585.

[17] S.A. El-Daly, S.M. Al-Hazmy, E.M. Ebeid, A.C. Bhasikuttan, D.K. Palit, A.V. Sapre, J.P. Mittal, Spectral, acid– base, and laser characteristics of 1, 4-Bis [β-(2-quinolyl) vinyl] benzene (BQVB), J. Phys. Chem. 100 (23) (1996) 9732–9737.

[18] S.M. Al-Hazmy, A.S. Babaqi, E. Daltrozzo, M. Klink, J. Sauter, E.M. Ebeid, A new diolefinic laser dye: 2, 5-bis-2-(2-naphthyl) vinyl pyrazine (B2NVP), J. Photochem. Photobiol. A Chem. 122 (1) (1999) 17–22.

[19] E.M. Ebeid, M.M.F. Sabry, S.A. El-Daly, 1, 4-Bis (β-Pyridyl-2-Vinyl) benzene (P2VB) and 2, 5-distyryl-pyrazine (DSP) as blue laser dyes, Laser Chem. 5 (4) (1985) 223–230.

[20] S.A. Azim, R. Ghazy, M. Shaheen, F. El-Mekawey, Investigations of energy transfer from some diolefinic laser dyes to Rhodamine 110, J. Photochem. Photobiol. A Chem. 133 (3) (2000) 185–188.

[21] J. Thipperudrappa, D.S. Biradar, S.M. Hanagodimath, Simultaneous presence of static and dynamic component in the fluorescence quenching of Bis-MSB by CCl_4 and aniline, J. Lumin. 124 (1) (2007) 45–50.

[22] M. Swierczewska, S. Lee, X. Chen, The design and application of fluorophore–gold nanoparticle activatable probes, PCCP 13 (2011) 9929–9941.

[23] K.G. Thomas, P.V. Kamat, Chromophore-functionalized gold nanoparticles, Acc. Chem. Res. 36 (12) (2003) 888–898.

[24] J. Zhang, E. Matveeva, I. Gryczynski, Z. Leonenko, J.R. Lakowicz, Metal-enhanced fluoroimmunoassay on a silver film by vapor deposition, J. Phys. Chem. B 109 (16) (2005) 7969–7975.

[25] C.F. Landes, M. Braun, M.A. El-Sayed, On the nanoparticle to molecular size transition: fluorescence quenching studies, J. Phys. Chem. B 105 (43) (2001) 10554–10558.

[26] E. Ciotta, P. Prosposito, R. Pizzoferrato, Positive curvature in Stern-Volmer plot described by a generalized model for static quenching, J. Lumin. 206 (2019) 518–522.

[27] J. Zhang, Y. Fu, J.R. Lakowicz, Enhanced Förster resonance energy transfer (FRET) on a single metal particle, J. Phys. Chem. C 111 (1) (2007) 50–56.

[28] J.R. Lakowicz, Y. Shen, S. D'Auria, J. Malicka, J. Fang, Z. Gryczynski, I. Gryczynski, Radiative decay engineering: 2. Effects of silver island films on fluorescence intensity, lifetimes, and resonance energy transfer, Anal. Biochem. 301 (2) (2002) 261–277.

[29] J. Zhang, Y. Fu, M.H. Chowdhury, J.R. Lakowicz, Metal-enhanced single-molecule fluorescence on silver particle monomer and dimer: coupling effect between metal particles, Nano Lett. 11, 7, 7 (2007) 2101–2107.

[30] C.C. You, O.R. Miranda, B. Gider, P.S. Ghosh, I.B. Kim, B. Erdogan, S.A. Krovi, U.H. Bunz, V.M. Rotello, Detection and identification of proteins using nanoparticle–fluorescent polymer 'chemical nose'sensors, Nat. Nanotechnol. 2 (5) (2007) 318–323.

[31] F. Suzuki, Y. Suzuki, H. Nakanishi, M. Hasegawa, Four-center type photopolymerization in the solid state. III. Polymerization of phenylene diacrylic acid and its derivatives, J. Polym. Sci. Part A-1 Polym. Chem. 7 (1969) 2319–2331.

[32] M.F. Abdelbar, H.S. El-Sheshtawy, K.R. Shoueir, I. El-Mehasseb, E.-Z. Ebeid, M. El-Kemary, Halogen bond triggered aggregation induced emission in an iodinated cyanine dye for ultra-sensitive detection of Ag nanoparticles in tap water and agricultural wastewater, RSC Adv. 8 (43) (2018) 24617–24626.

[33] S.K. Vaishanav, J. Korram, R. Nagwanshi, I. Karbhal, L. Dewangan, K.K. Ghosh, M.L. Satnami, Interaction of folic acid with Mn^{2+} doped CdTe/ZnS quantum dots. In situ detection of folic acid, J. Fluoresc. 31 (4) (2021) 951–960.

[34] M.F. Abdelbar, T.A. Fayed, T.M. Meaz, T. Subramani, N. Fukata, E.M. Ebeid, Hybrid organic and inorganic solar cell

based on a cyanine dye and quantum dots, J. Photochem. Photobiol. A Chem. 375 (2019) 166–174.
[35] S. Bhuin, S. Halder, S.K. Saha, M. Chakravarty, Binding interactions and FRET between bovine serum albumin and various phenothiazine-/anthracene-based dyes: a structure–property relationship, RSC Adv. 11 (3) (2021) 1679–1693.
[36] A. Kaur, P. Kaur, S. Ahuja, Förster resonance energy transfer (FRET) and applications thereof, Anal. Methods 13 (5) (2021) 730.
[37] C.L. Christenholz, D.A. Obenchain, R.A. Peebles, S.A. Peebles, Rotational spectroscopic studies of C-H··· F interactions in the vinyl fluoride··· difluoromethane complex, J. Phys. Chem. A 118 (9) (2014) 1610–1616.
[38] M. Bourass, N. Komiha, O.K. Kabbaj, N. Wazzan, M. Chemek, M. Bouachrine, The photophysical properties and electronic structures of bis[1]benzothieno[6,7-d:6′,7′-d′]benzo[1,2-b:4,5-b′] dithiophene (BBTBDT) derivatives as hole-transporting materials for organic light-emitting diodes (OLEDs), New J. Chem. 43 (40) (2019) 15899–15909.
[39] S.A. El-Daly, K.A. Alamry, Spectroscopic investigation and photophysics of a D-π-A-π-D type styryl pyrazine derivative, J Fluoresc. 26 (2016) 163–176.
[40] A. Nirwan, A. Devi, V.D. Ghule, Assessment of density prediction methods based on molecular surface electrostatic potential, J. Mol. Model. 24 (7) (2018) 1–11.
[41] A.E. Reed, F. Weinhold, Natural bond orbital analysis of near-Hartree–Fock water dimer, J. Chem. Phys. 78 (1983) 4066–4073.
[42] T. Zhao, T. Li, Y. Liu, Silver nanoparticle plasmonic enhanced Förster resonance energy transfer (FRET) imaging of protein-specific sialylation on the cell surface, Nanoscale 9 (28) (2017) 9841–9847.
[43] W.F. Falco, A.M. Queiroz, J. Fernandes, E.R. Botero, E.A. Falcão, F.E. Guimarães, J.C. M'Peko, S.L. Oliveira, I. Colbeck, A.R. Caires, Interaction between chlorophyll and silver nanoparticles: a close analysis of chlorophyll fluorescence quenching, J. Photochem. Photobiol. A Chem. 15 (299) (2015) 203–209.
[44] A.A. Abo-Alhasan, S.A. El-Daly, M.M. El-Hendawy, S.H. El-Khalfy, E.M. Ebeid, Rapid induced aggregation of gold nanoparticles by diolefinic dyes, J. Nanomater. Mol. Nanotechnol. 3 (2014) 2–7.
[45] T.U. Tumkur, J.K. Kitur, C.E. Bonner, A.N. Poddubny, E.E. Narimanov, M.A. Noginov, Control of Förster energy transfer in the vicinity of metallic surfaces and hyperbolic metamaterials, Faraday Discuss. 178 (2015) 395–412.
[46] S. Hou, Y. Chen, D. Lu, Q. Xiong, Y. Lim, H. Duan, A self-assembled plasmonic substrate for enhanced fluorescence resonance energy transfer, Adv. Mater. 32 (8) (2020) 1906475.